Accurately Modeling the Recovery Time of Superconducting Nanowire Single-Photon Detectors as a Function of Bias Current

Leo Oshiro[a], Hudson Jones[a], Tim Rambo[a], Josh Cassada[a], Stephanie Boyd[a], and Aaron Miller[a]

[a]Quantum Opus, LLC, 14841 Keel St., Plymouth, United States

ABSTRACT

Superconducting nanowire single-photon detectors (SNSPDs) are an attractive technology for applications which benefit from high-count rate photon detection such as quantum communication protocols, photon-starved classical communications, metrology of single-emitters, and photonic quantum computing. However, at high-count rates, a significant portion of photons may be incident during recovery intervals following prior detection events. After detection, the device efficiency recovers over nanoseconds to tens of nanoseconds before reaching a steady-state value. Therefore, for a given SNSPD bias current setpoint, a single efficiency and recovery time specification may not be sufficient to characterize the performance of a device at high count rates. Here we present and experimentally validate a model of the recovery time as a function of bias current for any given system efficiency. These results may be used to improve analysis of measurements performed using SNSPDs operating in the high count rate regime.

Keywords: Recovery time, superconducting nanowire single-photon detector (SNSPD), single-photon, detector, superconducting, photonics

1. INTRODUCTION

Single-photon detectors are essential components for many applications including fluorescence lifetime measurements,[1] LIDAR systems,[2] biomedical optics[3] as well as wide variety of quantum optics applications including quantum key distribution,[4] optical quantum computing,[5] and quantum networking.[6] SNSPDs are particularly useful for single-photon detector applications that require a low dark count rate,[7] high detection efficiency,[8,9] good timing resolution,[10] or quick recovery times.[11] An already established method of determining the recovery time involves observing how the count rates measured by the device change as one increases the incident count rate of a Poisson light source.[12] This method models the recovery of the device as an instantaneous reset after detection, obfuscating the fact that the device is in a state of partial recovery for nanoseconds to tens of nanoseconds. Another method of determining recovery time involves taking hybrid autocorrelation data using a high-flux pulsed laser and low-flux continuous wave (CW) laser and characterizing the recovery time from the resulting histogram.[13] One can use this method to determine recovery times for a single set bias. Here we present an autocorrelation method of recovery time characterization that can be used to determine recovery time to any arbitrary percentage of steady-state detection efficiency for any bias at which the device is active before intrinsic noise counts dominate.

2. MODEL

The inter-arrival times of a process are the collection of time differences between successive arrival events in the process. Similarly, we define the inter-detection times of a process as the collection of time differences between successive detection events in the process. In the case of photon detection, arrival events are events where a photon is incident on a photon detector whether or not it is detected and detection events are events when a photon is incident on the device and detected.

Further author information: (Send correspondence to H.J.)
H.J.: E-mail: hudson@quantumopus.com, Telephone: +1 (734) 228-4842
L.O.: E-mail: leo@quantumopus.com, Telephone: +1 (734) 228-4842 x215

The probability density function (PDF) for Poisson inter-arrival events is

$$f_{\mathrm{IAT}}(t) = \begin{cases} \lambda e^{-\lambda t}, & t > 0, \\ 0, & t < 0, \end{cases} \tag{1}$$

where λ is the mean arrival rate from the source and t is the time difference between successive arrival events. One can use a CW laser or thermal source attenuated sufficiently to act as the Poisson process in our model.[14] The PDF for inter-detection events is

$$f_{\mathrm{IDT}}(t) = \lambda \eta(t) \exp\left(-\lambda \int_0^t dt' \, \eta(t')\right), \quad t > 0, \tag{2}$$

where t is the time difference between successive detection events and $\eta(t)$ is the instantaneous efficiency of the detector.

2.1 Bias Current Recharge

When an SNSPD is in its superconducting state, it acts as an inductor with kinetic inductance L_{k} and has no resistance. When a photon is absorbed, the additional energy breaks the superconductivity and the SNSPD has some resistance, R. Additionally, following a photon absorption, the bias current through the device is i_{drop} and increases with the time constant $\tau = L_{\mathrm{k}}/R$.[15] The model we use for the current recharge is

$$i(t) = (i_{\mathrm{b}} - i_{\mathrm{drop}})(1 - e^{-t/\tau}) + i_{\mathrm{drop}}, \tag{3}$$

where $i(t)$ is the bias current through the device as a function of time after the detection event, i_{b} is the set bias current, and i_{drop} is the bias current in the device immediately after a detection event.

2.2 Efficiency vs. Bias Current

Dark counts describe the counts detected when there is no optical input to a detector. At low set bias, the dark counts are dominated by background thermal radiation, while at high set bias, they are dominated by the intrinsic thermal noise of the device.[16] The steady-state detection efficiency of an SNSPD is achieved when $i(t) \approx i_{\mathrm{b}}$. The steady-state detection efficiency as a function of set bias current follows an S-shaped curve. Measurements of the detection efficiency are limited by the intrinsic thermal noise of the device, which dominates over counts from light sources at high enough set bias. Thus, for bias currents below where intrinsic thermal noise dominates, we may model the normalized efficiency of the detector as a function of set bias current using

$$\eta(i) = \frac{\eta_0}{2}\left(1 + \mathrm{erf}(k(i - i_0))\right) \tag{4}$$

where i is the set bias current, $\eta_0 \in (0, 1]$ is the maximum efficiency of the detector, i_0 is the midpoint of the sigmoid, and k is a parameter which describes the steepness of the sigmoid.[17]

2.3 Instantaneous Efficiency

The composition of Equation 4 with Equation 3 gives the instantaneous normalized efficiency of the SNSPD after a detection event, which can be written:

$$\eta(t) \coloneqq \eta(i(t)). \tag{5}$$

With this general form and Equation 2 we may determine the free parameters using a fitting routine on data collected from a single-start single-stop histogram. The free parameters may then be used to determine the recovery times for any arbitrary recovery percentage using the inverse of Equation 5.

3. MEASUREMENTS AND RESULTS

In order to validate our model for the inter-detection time distribution, we first performed measurements to determine the efficiency as a function of set bias current. To do this, we attenuated a 1550 nm CW laser to 100 000 – 300 000 photons per second so that the probability of a photon being incident on the device during recovery is low. A power meter was used to measure the base and attenuated power of the laser, and the polarization was optimized at the device. Finally, while sweeping the set bias current, we recorded the count rate measured by the SNSPD and used the calibrated power to normalize the count rates into efficiencies. Figure 1 shows the resulting data along with dark counts. To obtain the wavelength-dependent free parameters of Equation 2 (η_0, i_0, and k), the resulting efficiency data was fit to Equation 4.

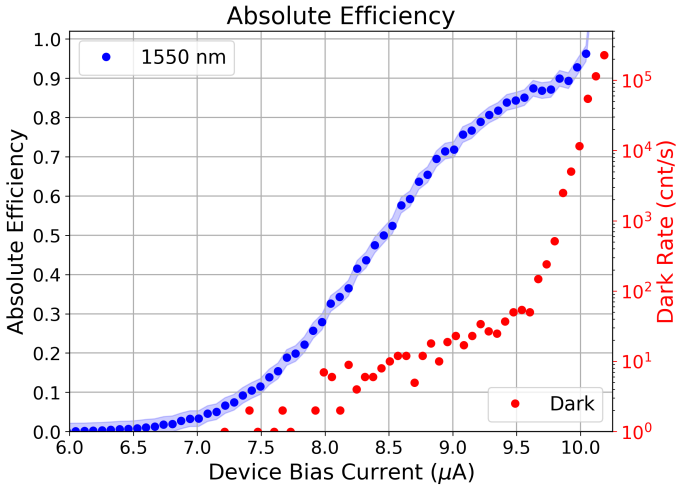

Figure 1. Measurement result of efficiency and dark count rate as a function of set bias current. The sigmoid shape is apparent until the intrinsic dark counts increase exponentially.

3.1 Direct Sampling

Using the same 1550 nm CW laser from the efficiency measurement, we attenuated laser power until an average measured rate of 1 million counts per second was observed. We then sampled the inter-detection distribution using a time tagger with 1 ps resolution connected to the electrical output of the device and put the data into a histogram as shown in Figure 2. The measured histogram was fit to Equation 2 multiplied by a scaling factor with fixed parameter values (η_0, i_0, and k) obtained by fitting the efficiency data. Finally, the resulting fit gave the wavelength-independent free parameters (A, λ, τ, and i_{drop}, where A is the scaling factor). The recovery times listed in Figure 2 were determined by evaluating $\eta(t)$ using the parameter values found in the fits.

3.2 Set Bias Current Dependence

One method to tune the performance of an SNSPD is by adjusting the set bias current. The set bias current can affect the steady state efficiency, dark count rate, recovery time, and jitter, so knowing these specifications at a range of set bias currents is valuable. We use the inverse of Equation 5 to determine the recovery time of an arbitrary efficiency recovery percentage. Equation 5 depends on i_{b} as seen in Equation 3 and therefore so does recovery time. By determining $\eta(t)$ from the sampling described in Section 3.1 for a chosen i_{b}, we have determined the necessary free parameters to extrapolate the recovery time for an arbitrary set bias current in addition to an arbitrary efficiency recovery percentage. The results of the modeled extrapolation using data acquired at a set bias current of 9.9 µA are shown in Figure 3 along with results obtained by performing the same sampling method and analysis described in Section 3.1 over a range of set bias currents.

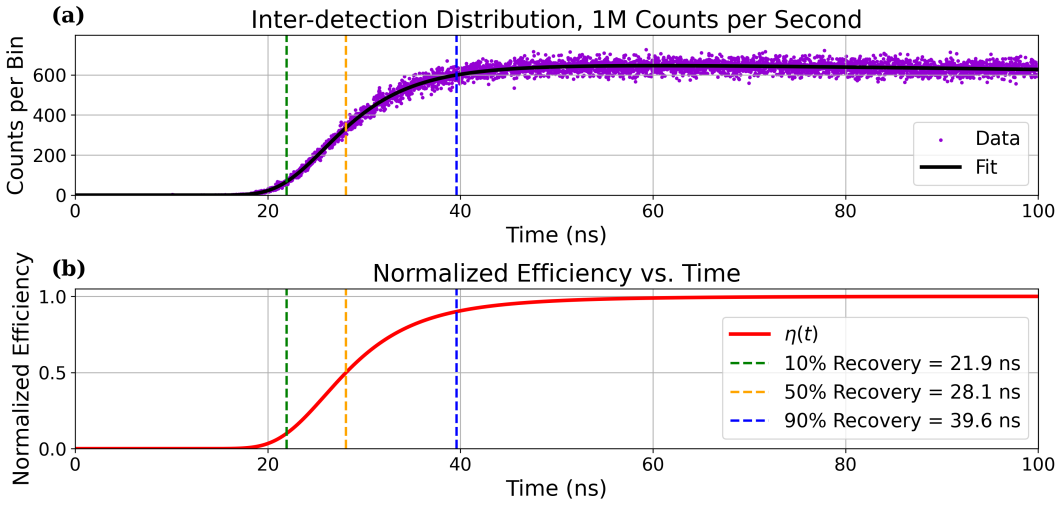

Figure 2. (a) Histogram of sampled inter-detection times with a 20 ps bin-width. Data was taken using a 1550 nm CW laser attenuated to around 1 million counts per second. A fit was performed to obtain the values needed to determine $\eta(t)$. (b) The efficiency vs. time normalized to the steady-state efficiency.

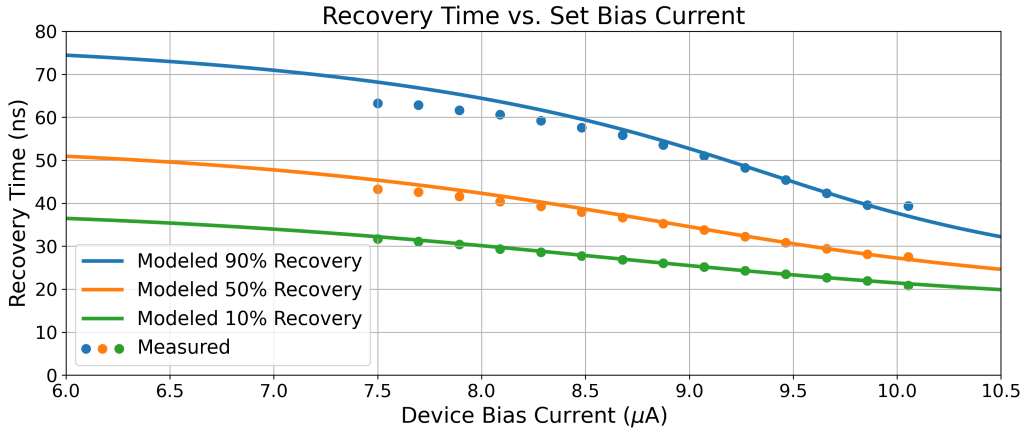

Figure 3. Estimated recovery times for a range of set bias currents and measured results. The recovery percentages are the same as those shown in Figure 2.

4. CONCLUSION

In this manuscript, we have presented an experimental method and analysis to characterize the recovery time of an SNSPD using a CW source. Compared to measurements of count-rate vs. incident power, our analysis reveals the full path of device recovery, which allows us to specify recovery times for any recovery level. By sampling the inter-detection distribution directly, we are able to experimentally extract $\eta(t)$ and use the results to predict recovery times for other set bias currents. Our analysis can be used to clarify the meaning of recovery time when discussing technical specifications of commercial SNSPDs.

REFERENCES

[1] Isbaner, S., Karedla, N., Ruhlandt, D., Stein, S. C., Chizhik, A., Gregor, I., and Enderlein, J., "Dead-time correction of fluorescence lifetime measurements and fluorescence lifetime imaging," *Opt. Express* **24**, 9429–9445 (May 2016).

[2] Hong, Y., Liu, S., Li, Z.-P., Huang, X., Jiang, P., Xu, Y., Wu, C., Zhou, H., Zhang, Y.-C., Ren, H.-L., Li, Z.-H., Jia, J., Zhang, Q., Li, C., Xu, F., Wang, J.-Y., and Pan, J.-W., "Airborne single-photon lidar towards a small-sized and low-power payload," *Optica* **11**, 612–618 (May 2024).

[3] Liu, Y., Yao, C.-Y., Rambo, T. M., Li, B., Juhong, A., Doredla, J. S., Luker, G. D., Han, M., Miller, A. J., and Qiu, Z., "Superconducting nanowire single-photon detector enhanced near-infrared ii portable confocal microscopy for tissue imaging with indocyanine green," *Opt. Lett.* **49**, 6349–6352 (November 2024).

[4] Zahidy, M., Mikkelsen, M., Müller, R., Da Lio, B., Krehbiel, M., Wang, Y., Bart, N., Wieck, A., Ludwig, A., Galili, M., Forchhammer, S., Lodahl, P., Oxenløwe, L., Bacco, D., and Midolo, L., "Quantum key distribution using deterministic single-photon sources over a field-installed fibre link," *npj Quantum Information* **10**(1) (2024).

[5] Maring, N., Fyrillas, A., Pont, M., Ivanov, E., Stepanov, P., Margaria, N., Hease, W., Pishchagin, A., Lemaître, A., Sagnes, I., Au, T. H., Boissier, S., Bertasi, E., Baert, A., Valdivia, M., Billard, M., Acar, O., Brieussel, A., Mezher, R., Wein, S. C., Salavrakos, A., Sinnott, P., Fioretto, D. A., Emeriau, P.-E., Belabas, N., Mansfield, S., Senellart, P., Senellart, J., and Somaschi, N., "A versatile single-photon-based quantum computing platform," *Nature Photonics* **18**, 603–609 (2024).

[6] Knaut, C. M., Suleymanzade, A., Wei, Y.-C., Assumpcao, D. R., Stas, P.-J., Huan, Y. Q., Machielse, B., Knall, E. N., Sutula, M., Baranes, G., Sinclair, N., De-Eknamkul, C., Levonian, D. S., and Bhas, M. K., "Entanglement of nanophotonic quantum memory nodes in a telecom network," *Nature* **629**, 573–578 (May 2024).

[7] Shibata, H., Shimizu, K., Takesue, H., and Tokura, Y., "Ultimate low system dark-count rate for superconducting nanowire single-photon detector," *Opt. Lett.* **40**, 3428–3431 (Jul 2015).

[8] Reddy, D. V., Nerem, R. R., Nam, S. W., Mirin, R. P., and Verma, V. B., "Superconducting nanowire single-photon detectors with 98% system detection efficiency at 1550nm," *Optica* **7**, 1649–1653 (December 2020).

[9] Hu, P., Li, H., You, L., Wang, H., Xiao, Y., Huang, J., Yang, X., Zhang, W., Wang, Z., and Xie, X., "Detecting single infrared photons toward optimal system detection efficiency," *Opt. Express* **28**, 36884–36891 (November 2020).

[10] Korzh, B., Zhao, Q., Allmaras, J., Frasca, S., Autry, T., Bersin, E., Beyer, A., Briggs, R., Bumble, B., Colangelo, M., Crouch, G., Dane, A., Gerrits, T., Lita, A., Marsili, F., Moody, G., Pena, C., Ramirez, E., Rezac, J., and Berggren, K., "Demonstration of sub-3 ps temporal resolution with a superconducting nanowire single-photon detector," *Nature Photonics* **14**, 250–255 (April 2020).

[11] Lv, C., Zhang, W., You, L., Hu, P., Wang, H., Li, H., Zhang, C., Huang, J., Wang, Y., Yang, X., Wang, Z., and Xie, X., "Improving maximum count rate of superconducting nanowire single-photon detector with small active area using series attenuator," *AIP Advances* **8**, 105018 (October 2018).

[12] Usman, S. and Patil, A., "Radiation detector deadtime and pile up: A review of the status of science," *Nuclear Engineering and Technology* **50**, 1006–1016 (October 2018).

[13] Autebert, C., Gras, G., Amri, E., Perrenoud, M., Caloz, M., Zbinden, H., and Bussières, F., "Direct measurement of the recovery time of superconducting nanowire single-photon detectors," *Journal of Applied Physics* **128**, 4504 (August 2020).

[14] Hu, Y., Peng, X., Li, T., and Guo, H., "On the poisson approximation to photon distribution for faint lasers," *Physics Letters A* **367**(3), 173–176 (2007).

[15] Kerman, A., Yang, J., Molnar, R., Dauler, E., and Berggren, K., "Electrothermal feedback in superconducting nanowire single-photon detectors," *Physical Review B* **79** (December 2008).

[16] Shehata, A. B., Ruggeri, A., Stellari, F., Weger, A. J., Song, P., Sunter, K., Najafi, F., Berggren, K. K., and Anant, V., "Effect of temperature on superconducting nanowire single-photon detector noise," in [*Optical Sensing, Imaging, and Photon Counting: Nanostructured Devices and Applications*], Razeghi, M., Temple, D. S., and Brown, G. J., eds., **9555**, 95550C, International Society for Optics and Photonics, SPIE (2015).

[17] Verma, V. B., Korzh, B., Bussières, F., Horansky, R. D., Dyer, S. D., Lita, A. E., Vayshenker, I., Marsili, F., Shaw, M. D., Zbinden, H., Mirin, R. P., and Nam, S. W., "High-efficiency superconducting nanowire single-photon detectors fabricated from mosi thin-films," *Opt. Express* **23**, 33792–33801 (December 2015).